Eur. Phys. J. Appl. Phys. **86**, 30101 (2019)

https://doi.org/10.1051/epjap/2019190124

THE EUROPEAN PHYSICAL JOURNAL APPLIED PHYSICS

Regular Article

A numerical model of electrical characteristics for the monolayer graphene field effect transistors

Xiang-Jie Xiao, Piao-Rong Xu*, Gen-Hua Liu, Hui-Ying Zhou, Jian-Jun Li, Ai-Bin Chen, Yong-Zhong Zhang, and Hong-Xu Huang

College of Computer and Information Engineering, Central South University of Forestry and Technology, Changsha 410004, PR China

Received: 11 April 2019 / Received in final form: 8 June 2019 / Accepted: 12 June 2019

Abstract. A numerical model of carrier saturation velocity and drain current for the monolayer graphene field effect transistors (GFETs) is proposed by considering the exponential distribution of potential fluctuations in disordered graphene system. The carrier saturation velocity of GFET is investigated by the two-region model, and it is found to be affected not only by the carrier density, but also by the graphene disorder. The numerical solutions of the carrier density and carrier saturation velocity in the disordered GFETs yield clear and physical-based results. The simulated results of the drain current model show good consistency with the reported experimental data.

1 Introduction

In recent years, graphene has emerged as a novel material for applications in high-performance nano-electronic devices. Comparing with typical semiconductors like Si and InGaZnO [1,2], graphene possesses two dimensional (2D) nature, very high carrier mobility, zero band gap and ambipolar behavior [3,4]. Based on these advantages, extensive attentions have been dedicated to graphene for applications in flexible display, sensor and high frequency device, especially radio frequency device.

Monolayer graphene (MLG) has zero bandgap and unique linear chiral Dirac carrier dispersion relation. Many researchers investigated the drain-source current model of MLG based on the linear dispersion and provided proper reproduction of current-voltage characteristics for experimentally fabricated graphene field effect transistors (GFETs) [5,6], but with the carrier saturation velocity (υ_{sat}) significantly overestimated when the carrier density is small. Meanwhile, the inevitablely presented impurities lead to the formation of inhomogeneous electron-hole puddles [7–9], therefore the linear Dirac carrier dispersion breaks up into a disordered graphene system in MLG [10–15]. The effects of disorder on the quantum capacitance and carrier density of graphene devices have been studied for the first time using a Gaussian distribution of the potential fluctuations [13–15]. The exponential distribution model is an approximation of the physics-based Gaussian model which leads to analytical expression for quantum capacitance and drain-source current [10–12]. It is illustrated that the potential fluctuation function of the exponential distribution is valid in disordered systems.

Usually the saturation velocity is modeled as inversely proportional to the channel carrier density ($\propto\rho^{-\frac{1}{2}}$) of graphene [5,16]. This approximation can provide accurate υ_{sat} at high ρ, but is very inaccurate for low ρ (infinite υ_{sat}). Therefore, a two-region model was proposed to correct infinite υ_{sat} at low ρ based on Landauer transport theory [17], in which υ_{sat} is limited at low carrier density. However, the model in reference [17] is based on linear chiral Dirac carrier dispersion relation, which ignores the specific effects of the disorder on υ_{sat} in graphene system. The material disorder affects the density of states (DOS) distribution in GFETs, and therefore affects ρ and υ_{sat}. It's worth noting that the effect of disorder on υ_{sat} at low channel carrier density is usually based on the fitting of the relevant parameters [11,18], which lacks specific physical meaning.

In this work, the influence of material disorder on carrier saturation velocity and current-voltage characteristics based on the exponential distribution for potential fluctuations is analyzed. The numerical solution of the carrier saturation velocity is calculated using the two-region model, more accurate and physical-based results are yielded in disordered graphene system. These approaches can reproduce the current-voltage characteristics of experimental GFETs properly.

2 Model

Figure 1 shows the typical structure of a top-gate monolayer GFET with channel length L. The source is grounded and the drain-source voltage V_{ds} can be applied to the drain with potential drop $V(x)$ inside the channel. The potential difference between the channel and the gate controls the density and type of carriers in the GFET channel.

* e-mail: xprolive@126.com

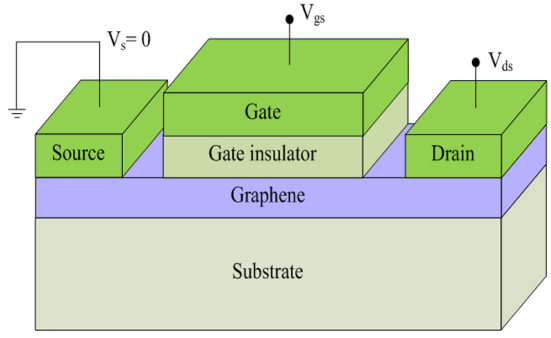

Fig. 1. The schematic diagram of GFET.

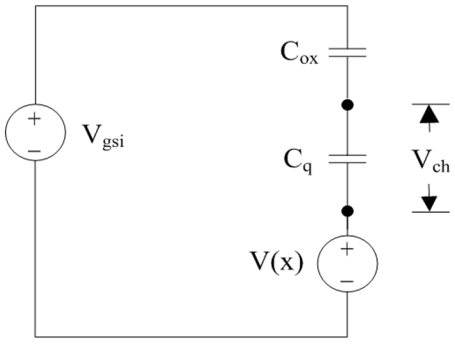

Fig. 2. Equivalent capacitive circuit of the GFET.

In general, the drain current $I_{\rm ds}$ of GFET can be expressed as:

$$I_{\rm ds} = -q\rho_{\rm sh}\upsilon W \tag{1}$$

where q is the elementary charge, $\rho_{\rm sh}$ is the carrier density in the channel, υ the carrier drift velocity, and W the gate width. In the following, by considering material disorder, more accurate expressions are proposed to properly describe the carrier density and the carrier velocity.

2.1 Carrier density $\rho_{\rm sh}$

For graphene, the potential fluctuations induced by unintended charged impurities can be described by the exponential distribution [10]:

$$P(V) = \begin{cases} \dfrac{1}{2\sigma} e^{\dfrac{V}{\sigma}} & V < 0 \\ \dfrac{1}{2\sigma} e^{-\dfrac{V}{\sigma}} & V > 0 \end{cases} \tag{2}$$

where V is the fluctuating potential energy, σ is the exponential disorder parameter, which manifests the strength of the potential fluctuation. Based on equation (2), a non-linear density of states per unit area of electrons is obtained:

$$\begin{aligned} D(E) &= \int_{-\infty}^{E} D_1(E-V)P(V)dV \\ &= \begin{cases} D_1\left(E + \dfrac{\sigma}{2} e^{-\dfrac{E}{\sigma}}\right) & E > 0 \\ D_1 \dfrac{\sigma}{2} e^{\dfrac{E}{\sigma}} & E < 0 \end{cases} \end{aligned} \tag{3}$$

where $D_1 = \frac{2}{\pi(\hbar\upsilon_f)^2}$, $\hbar$ is the reduced Planck constant, υ_f is the Fermi velocity equaling to 10^8 cm/s. Meanwhile, DOS per unit area for holes can be expressed as $D(-E)$, where E is the energy and $E = 0$ is the conduction band minimum.

Generally, the carrier density is calculated using numerical integration of the DOS and the Fermi–Dirac distribution. Therefore, the calculation of carrier density which contains the non-disorder part n_0 and the disorder part $n_{\rm dis}$ for electrons can be obtained as:

$$\begin{aligned} n_e &= n_0 + n_{\rm dis} = \int_{-\infty}^{\infty} D(E)f(E)dE \\ &= D_1 \int_0^{\infty} Ef(E)dE \\ &\quad + D_1\left(\int_0^{\infty} \frac{\sigma}{2} e^{-\frac{E}{\sigma}} f(E)dE + \int_{-\infty}^{0} \frac{\sigma}{2} e^{\frac{E}{\sigma}} f(E)dE\right) \end{aligned} \tag{4}$$

where the first term denotes the non-disorder part of the carrier density, the second term denotes the part induced by disorder. And $f(E)$ is the Fermi–Dirac occupation function, expressed as $f(E) = \frac{1}{1+e^{\frac{E-E_F}{\beta}}}$, where $\beta = kT$, T is the temperature, k is the Boltzmann constant, E_F is the Fermi energy. Due to the symmetry characteristic of graphene, only the electron branch ($E_F > 0$) is discussed here. The carrier density $\rho_{\rm sh}$ and quantum capacitance C_q are derived as [10]:

$$\begin{aligned} \rho_{\rm sh} &= \frac{1}{6} D_1 \left(-\left(6\sigma^2 + \pi^2\beta^2\right) e^{-\frac{E_F}{\beta}} + 6\pi\beta\sigma \csc\left(\frac{\pi\beta}{\sigma}\right)\right. \\ &\quad \left. \times \left(e^{-\frac{E_F}{\beta}} - e^{-\frac{E_F}{\sigma}}\right) + 3E_F^2 + \pi^2\beta^2 + 6\sigma^2\right) \end{aligned} \tag{5}$$

$$\begin{aligned} C_q &= -\frac{dQ_{\rm sh}}{dE_F} = \frac{D_1 q}{3}\left(\frac{\pi^2\beta^2 + 6\sigma^2}{\beta} e^{-\frac{E_F}{\beta}}\right. \\ &\quad \left. + 6\pi\left(e^{-\frac{E_F}{\sigma}}\beta - e^{-\frac{E_F}{\beta}}\sigma\right)\csc\left(\frac{\pi\beta}{\sigma}\right) + 6E_F\right) \end{aligned} \tag{6}$$

where $E_F = q \times V_{\rm ch}$ means the energy difference between the Fermi energy and the Dirac point, $V_{\rm ch}$ represents the voltage drop across C_q.

The equivalent capacitive circuit of the top-gate GFET is depicted in Figure 2. The channel potential $V(x)$ is zero at $x = 0$ and equals to the drain-source voltage $V_{\rm DS}$ at $x = L$. The dependency of C_q on voltage drop $V_{\rm ch}$ in graphene can be evaluated by introducing a capacitance weighting factor 0.5 [11,19], thus we get the

overall net mobile charge density:

$$Q_{\rm sh} = -\frac{1}{2}C_q V_{\rm ch.} \tag{7}$$

Applying Kirchhoff's laws to the equivalent circuit from Figure 2, the expression of $V_{\rm ch}$ can be derived as:

$$V_{\rm ch} = (V_{\rm gs} - V(x) - V_{\rm gs0})\frac{C_{\rm ox}}{C_{\rm ox} + \frac{1}{2}C_q} \tag{8}$$

where $C_{\rm ox}$ is the top-gate oxide capacitance, $V_{\rm gs0}$ is the top-gate voltage at the Dirac point. Connecting equation (6), equation (7) and equation (8), the relationship between the gate voltage $V_{\rm gs}$ and carrier density $\rho_{\rm sh}$ is obtained.

2.2 The carrier velocity υ

The carrier drift velocity υ depends on saturation velocity $\upsilon_{\rm sat}$ [20,21], and can be approximated as:

$$\upsilon = \frac{\mu E}{1 + \frac{\mu|E|}{\upsilon_{\rm sat}}} \tag{9}$$

where μ is the low-field mobility, E the electric field. The Landauer transport model [22] is used with assuming zero temperature, and positive gate bias and drain-source voltage $V_{\rm ds}$ are applied to the graphene field effect transistor. Under this circumstance, an electric field E is formed, which changes the k vectors of the electrons, leading to the states at $-k_x$ being emptied and the states at $+k_x$ being filled. The energy level $E_F{}^+$ and $E_F{}^-$ ($E_F{}^+$ locates above $E_F{}^-$) correspond to the filled $+k_x$ and $-k_x$ states, respectively. An effective energy $\hbar\Omega$ of one phonon between $E_F{}^+$ and $E_F{}^-$ is applied to describe the major interfacial phonon scattering in graphene located on SiO_2 [17,20,23,24]. Under steady-state conditions the difference between $E_F{}^+$ and $E_F{}^-$ could never be larger than $\hbar\Omega$, otherwise an optical phonon could be emitted.

As shown in Figure 3, there are three cases for the large non-equilibrium between $+k_x$ and $-k_x$ state: ① for large $\rho_{\rm sh}$, $E_F{}^+$ and $E_F{}^-$ are both positive; ② as $\rho_{\rm sh}$ decreases to a critical carrier density $\rho_{\rm cr}$, $E_F{}^-$ decrease to zero at some point; ③ as $\rho_{\rm sh}$ further decreases, $E_F{}^-$ becomes negative. Therefore the current would saturate, which can be calculated with corresponding saturation velocity by the Landauer transport formula. It is worth mentioning that although Landauer transport model is used for zero temperature, here Fermi function can be approximated to Heaviside function at the situation $\hbar\Omega \gg kT$ [25], which simplifies the integration for the carrier density.

$$I_{\rm sat} = q\rho^*_{\rm sh}\upsilon_{\rm sat}W = qW\frac{2\upsilon_f}{\pi}\int_{E_0}^{E_0+\hbar\Omega} D(E)dE \tag{10}$$

where $\rho^*_{\rm sh}$ is the nonequilibrium density of carriers, W is the channel width, $E_F{}^- = E_0$, $E_F{}^+ = E_0 + \hbar\Omega$. Note that for small gate bias $\rho^*_{\rm sh}$ becomes very different from $\rho_{\rm sh}$ because strong electric fields in $-x$ direction can promote electrons

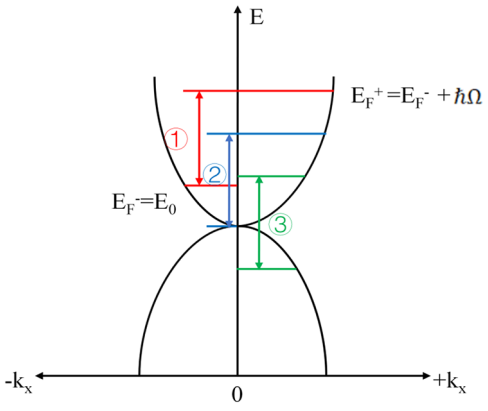

Fig. 3. Occupation of the conduction band states in large non-equilibrium between $+k_x$ and $-k_x$ states: ① for large $\rho_{\rm sh}$, $E_F{}^+$ and $E_F{}^-$ are both positive; ② as $\rho_{\rm sh}$ decreases to a critical carrier density $\rho_{\rm cr}$, $E_F{}^-$ decrease to zero; ③ for low $\rho_{\rm sh}$, $E_F{}^+$ is positive, $E_F{}^-$ becomes negative.

from the $-k_x$ states in the valence band into the $+k_x$ states in conduction band and therefore produce additional electrons and holes. In the first situation, $\rho_{\rm sh}$ is large enough so that $E_F{}^+$ and $E_F{}^-$ are both positive. At this time $\rho_{\rm sh} = \rho^*_{\rm sh}$, and can be calculated by:

$$\begin{aligned}\rho_{\rm sh} = \rho^*_{\rm sh} = \frac{D_1}{2}\Bigg(&\int_0^{E_0}\left(E + \frac{\sigma}{2}e^{-\frac{E}{\sigma}}\right)dE \\ &+ \int_0^{E_0+\hbar\Omega}\left(E + \frac{\sigma}{2}e^{-\frac{E}{\sigma}}\right)dE\Bigg) \\ = \frac{1}{2\pi(\hbar\upsilon_f)^2}\Bigg(&E_0^2 + (E_0+\hbar\Omega)^2 \\ &-\sigma^2\left(e^{-\frac{E_0+\hbar\Omega}{\sigma}} + e^{-\frac{E_0}{\sigma}} - 2\right)\Bigg).\end{aligned} \tag{11}$$

The saturation current is calculated by equation (10):

$$\begin{aligned}I_{\rm sat} &= qW\frac{2\upsilon_f}{\pi}\int_{E_0}^{E_0+\hbar\Omega}\frac{D_1}{2}\left(E + \frac{\sigma}{2}e^{-\frac{E}{\sigma}}\right)dE \\ &= \frac{2qW}{(\pi\hbar)^2\upsilon_f}\left(E_0\hbar\Omega + \frac{(\hbar\Omega)^2}{2} - \frac{\sigma^2}{2}\left(e^{-\frac{E_0+\hbar\Omega}{\sigma}} - e^{-\frac{E_0}{\sigma}}\right)\right).\end{aligned} \tag{12}$$

Then, E_0 and $\upsilon_{\rm sat}$ can be obtained by numerical iterations.

$$\upsilon_{\mathrm{sat}} = \frac{I_{\mathrm{sat}}}{q\rho^{*}_{\mathrm{sh}}W} = \frac{4\upsilon_f}{\pi}\left(E_0\hbar\Omega + \frac{(\hbar\Omega)^2}{2} - \frac{\sigma^2}{2}\left(e^{-\frac{E_0+\hbar\Omega}{\sigma}} - e^{-\frac{E_0}{\sigma}}\right)\right) \Bigg/ \left(E_0^2 + (E_0+\hbar\Omega)^2 - \sigma^2\left(e^{-\frac{E_0+\hbar\Omega}{\sigma}} + e^{-\frac{E_0}{\sigma}} - 2\right)\right). \tag{13}$$

As the carrier density reduces, $E_F{}^{-}$ decreases and becomes zero at some point. The critical carrier density can be expressed as:

$$\rho_{\mathrm{cr}} = \frac{D_1}{2}\left(\int_0^{\hbar\Omega}\left(E + \frac{\sigma}{2}e^{-\frac{E}{\sigma}}\right)dE\right) = \frac{D_1}{4}\left((\hbar\Omega)^2 - \sigma^2\left(e^{-\frac{\hbar\Omega}{\sigma}} - 1\right)\right). \tag{14}$$

As we can see, further reduction of ρ_{sh} leads to negative $E_F{}^{-}$, and the current is carried by both electrons and holes.

$$\rho_{\mathrm{sh}} = \frac{D_1}{2}\left(\int_{E_0}^{0}\left(-E + \frac{\sigma}{2}e^{\frac{E}{\sigma}}\right)dE - \int_0^{E_0+\hbar\Omega}\left(E + \frac{\sigma}{2}e^{-\frac{E}{\sigma}}\right)dE\right) \tag{15}$$

where ρ^{*}_{sh} is the sum of electrons and holes:

$$\rho^{*}_{\mathrm{sh}} = \frac{D_1}{2}\int_{E_0}^{E_0+\hbar\Omega} D(E)dE = \frac{D_1}{2}\left(\int_{E_0}^{0}\left(-E + \frac{\sigma}{2}e^{\frac{E}{\sigma}}\right)dE + \int_0^{E_0+\hbar\Omega}\left(E + \frac{\sigma}{2}e^{-\frac{E}{\sigma}}\right)dE\right). \tag{16}$$

Connecting equation (10) and equation (16), the saturation velocity is expressed as:

$$\upsilon_{\mathrm{sat}} = \frac{I_{\mathrm{sat}}}{q\rho^{*}_{\mathrm{sh}}W} = \frac{2\upsilon_f}{\pi} \tag{17}$$

Then the carrier velocity υ is obtained by substituting equation (13) and equation (17) into equation (9). Eventually, the current I_{ds} can be calculated using equation (1), which can be rewritten as [11,19]:

$$I_{\mathrm{ds}} = \frac{\mu w q\int_0^{V_{\mathrm{ds}}}|\rho_{\mathrm{sh}}|dV}{L + \mu\left|\int_0^{V_{\mathrm{ds}}}\frac{1}{\upsilon_{sat}}dV\right|}. \tag{18}$$

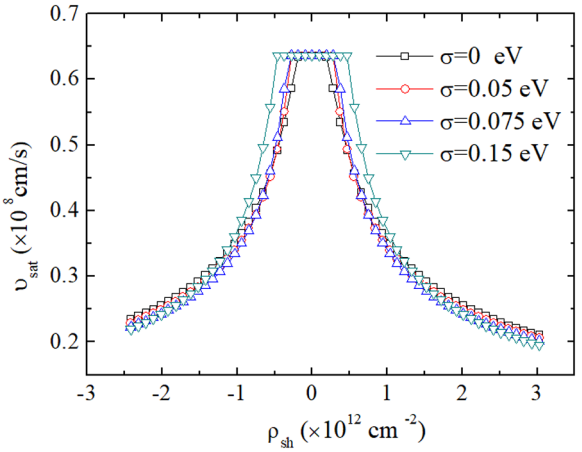

Fig. 4. Dependency of the carrier saturation velocity υ_{sat} on the carrier density with different potential fluctuation strength.

3 Results and discussions

The relation between the saturation velocity υ_{sat} and the carrier density ρ_{sh} considering the restrained saturation velocity under steady-state conditions in GFETs is shown in Figure 4. We can see that the saturation velocity is limited to $\frac{2\upsilon_f}{\pi}$ for small ρ_{sh} around the Dirac point, whether the graphene disorder is considered or not. As ρ_{sh} increases, υ_{sat} decreases, which is consistent with other reported results [5,16,17].

The DOS of graphene increases by considering the exponential distribution of potential fluctuations, therefore the carrier density is larger in disorder graphene system ($\sigma > 0$) than that in non-disorder ($\sigma = 0$) graphene system. Comparing the simulated results of the saturation velocity model between disorder and non-disorder graphene systems, we found that when the carrier density ρ_{sh} is small, the disorder part plays an important role in the DOS of graphene. And as potential fluctuation strength σ increases, the carrier density increases. Therefore according to the Fermi–Dirac occupation function, in order to keep a certain carrier density, E_0 is smaller in the disorder graphene, and increases at a descending series of σ. Therefore E_0 is more possible to be negative at high σ, as shown in Figure 5. When E_0 is negative, the corresponding saturation velocity υ_{sat} reaches its maximum value $\frac{2\upsilon_f}{\pi}$, and υ_{sat} is increased continuously, we can thus get larger υ_{sat} in the more disordered graphene at low ρ_{sh}, as shown in Figure 4. As the carrier density ρ_{sh} increases, the effect of disorder part on the exponential DOS becomes less obvious, and E_0 increases in both non-disorder and disorder graphene system, but the variation of energy difference for E_0 between the non-disorder and the disorder graphene system is not significant, as depicted in Figure 5. The small E_0 in disorder graphene becomes increasingly important, therefore the saturation velocity υ_{sat} decreases much more quickly, leading to an equivalent υ_{sat} in both non-disorder and disorder GFET. When the carrier density ρ_{sh} is larger, the relatively larger E_0 makes the disorder part approach to zero. The saturation velocity υ_{sat} in the disorder graphene

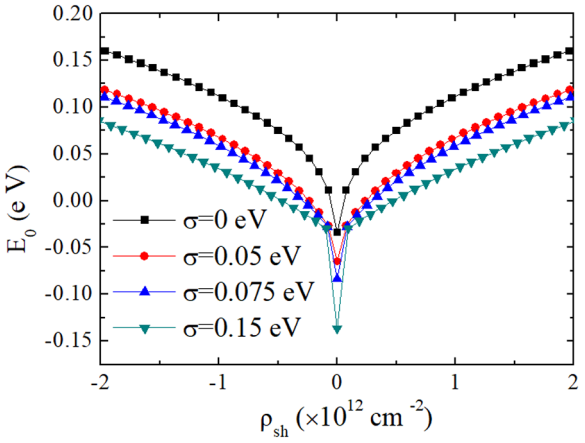

Fig. 5. Dependency of E_0 on the carrier density with different potential fluctuation strength.

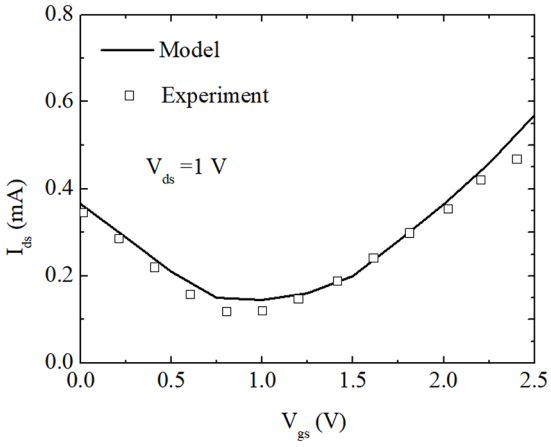

Fig. 7. Calculated transfer characteristics (full lines) and comparison with experimental data from reference [26] (symbols).

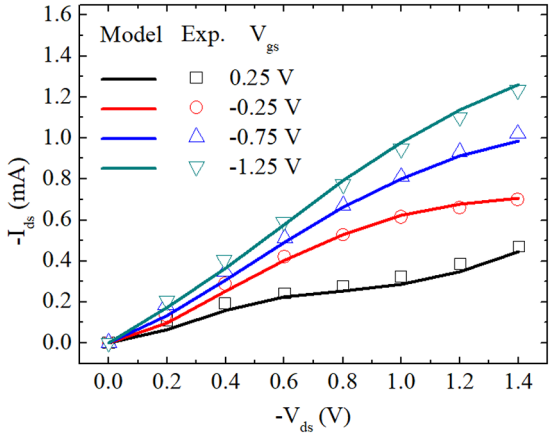

Fig. 6. Calculated output characteristics (full lines) and comparison with experimental data from reference [26] (symbols).

Table 1. Parameters used in the model.

Parameters	Description	Values
W (μm)	Channel width	5
L (μm)	Channel length	10
$t_{\text{ox-top}}$ (nm)	The thickness of the top-gate oxide	40
ε_{ox}	Relative dielectric constant	16
$V_{\text{GS-top0}}$ (V)	The top-gate voltage at the Dirac point	1
μ_{n} ($\text{cm}^2/\text{V s}$)	Electron mobility	6500
μ_{p} ($\text{cm}^2/\text{V s}$)	Hole mobility	6500
$\hbar\Omega$ (meV)	Phonon energy	68

system decreases to a value slightly lower than that in non-disorder graphene system, which is contributed to the decreasing of the saturation current with the energy difference for E_0.

In order to verify the validity of our model, we numerically simulated the output and the transfer characteristic of the GFET. The results are compared with experimental results in reference [26], as shown in Figures 6 and 7. In reference [26], a top-gate GFET with a thin graphene film and HfO_2 gate insulator is prepared. The GFET dimensions and the parameters used in the model are listed in Table 1. The comparison of our modeled drain current with the experimental results from reference [26] shows a good agreement.

4 Conclusion

In summary, a numerical model of drain current for monolayer GFET is established based on the exponential distribution of potential fluctuations for disordered graphene system. The simulated results are in accordance with the experiments. The developed saturation velocity is physically analyzed by considering the influence of graphene disorder based on Landauer transport theory, and is corrected for low channel carrier density, offering a good insight into the essential device physics of graphene. The model provides optimization of current-voltage characteristics for clear physical significance in GFET.

This work was supported by the Central South University of Forestry and Technology Foundation, China (Grant No. 0409-2016 and 0z85-2018).

References

1. C.C.-C. Chung et al., IEEE Trans. Electron Devices **65**, 756 (2018)
2. P.-R. Xu, R.-H. Yao, Eur. Phys. J. Appl. Phys. **72**, 30102 (2015)
3. K.S. Novoselov et al., Science **306**, 666 (2004)
4. L. Liao et al., Nature **467**, 305 (2010)

5. S. Fregonese et al., Solid-State Electr. **73**, 27 (2012)
6. S.A. Thiele, J.A. Schaefer, F. Schwierz, J. Appl. Phys. **107**, 094505 (2010)
7. S.D. Sarma et al., Rev. Mod. Phys. **83**, 407 (2011)
8. Q.Z. Li, E.H. Hwang, S.D. Sarma, Phys. Rev. B **84**, 115442 (2011)
9. Q.Z. Li et al., Phys. Rev. Lett. **107**, 156601 (2011)
10. L. Wang et al., Appl. Phys. Lett. **108**, 013503 (2016)
11. F. Zhuang et al., AIP Adv. **9**, 025222 (2019)
12. H.C.D. Lin et al., Microelectr. Eng. **147**, 314 (2015)
13. G.S. Kliros, Rom. J. Inf. Sci. Technol. **13**, 332 (2010)
14. M.A. Ebrish, H. Shao, S.J. Koester, Appl. Phys. Lett. **100**, 143102 (2012)
15. G.S. Kliros, Superlattices Microstruct. **52**, 1093 (2012)
16. D. Jiménez, O. Moldovan, IEEE Trans. Electron Devices **58**, 4049 (2011)
17. S. Thiele, F. Schwierz, J. Appl. Phys. **110**, 034506 (2011)
18. J.D. Aguirre-Morales et al., *45th European Solid-State Device Research Conference, ESSDERC* (2015)
19. S.A. Thiele, J.A. Schaefer, F. Schwierz, J. Appl. Phys. **107**, 094505 (2010)
20. V.E. Dorgan, M.-H. Bae, E. Pop, Appl. Phys. Lett. **97**, 082112 (2010)
21. R.S. Shishir, D.K. Ferry, J. Phys.: Condens. Matter **21**, 344201 (2009)
22. S. Datta, *Electronic Transport in Mesoscopic Systems* (Cambridge University Press, Cambridge, 2002)
23. I. Meric et al., Nat. Nanotechnol. **3**, 654 (2008)
24. J.-H. Chen et al., Solid State Commun. **149**, 1080 (2009)
25. D. Jena, J. Appl. Phys. **105**, 123701 (2009)
26. J. Kedzierski et al., IEEE Electron Device Lett. **30**, 745 (2009)

Cite this article as: Xiang-Jie Xiao, Piao-Rong Xu, Gen-Hua Liu, Hui-Ying Zhou, Jian-Jun Li, Ai-Bin Chen, Yong-Zhong Zhang, Hong-Xu Huang, A numerical model of electrical characteristics for the monolayer graphene field effect transistors, Eur. Phys. J. Appl. Phys. **86**, 30101 (2019)